Improved texture analysis for automatic detection of tuberculosis (TB) on chest radiographs with bone suppression images

Pragnya Maduskar, Laurens Hogeweg, Rick Philipsen, Steven Schalekamp and Bram van Ginneken

Diagnostic Image Analysis Group, Department of Radiology,
Radboud University Nijmegen Medical Centre, The Netherlands

ABSTRACT

Computer aided detection (CAD) of tuberculosis (TB) on chest radiographs (CXR) is challenging due to overlapping structures. Suppression of normal structures can reduce overprojection effects and can enhance the appearance of diffuse parenchymal abnormalities. In this work, we compare two CAD systems to detect textural abnormalities in chest radiographs of TB suspects. One CAD system was trained and tested on the original CXR and the other CAD system was trained and tested on bone suppression images (BSI). BSI were created using a commercially available software (ClearRead 2.4, Riverain Medical). The CAD system is trained with 431 normal and 434 abnormal images with manually outlined abnormal regions. Subtlety rating (1-3) is assigned to each abnormal region, where 3 refers to obvious and 1 refers to subtle abnormalities. Performance is evaluated on normal and abnormal regions from an independent dataset of 900 images. These contain in total 454 normal and 1127 abnormal regions, which are divided into 3 subtlety categories containing 280, 527 and 320 abnormal regions, respectively. For normal regions, original/BSI CAD has an average abnormality score of 0.094±0.027/0.085±0.032 ($p = 5.6\times10^{-19}$). For abnormal regions, subtlety 1, 2, 3 categories have average abnormality scores for original/BSI of 0.155±0.073/0.156±0.089 ($p = 0.73$), 0.194±0.086/0.207±0.101 ($p = 5.7\times10^{-7}$), 0.225±0.119/0.247±0.117 ($p = 4.4\times10^{-7}$), respectively. Thus for normal regions, CAD scores slightly decrease when using BSI instead of the original images, and for abnormal regions, the scores increase slightly. We therefore conclude that the use of bone suppression results in slightly but significantly improved automated detection of textural abnormalities in chest radiographs.

Keywords: Bone suppression, CAD, Chest X-ray, Radiograph, Tuberculosis

1. PURPOSE

Chest radiographs (CXR) are difficult to interpret due to the presence of overlapping structures on a 2D projection image. Visibility of abnormalities on CXR is sometimes hampered by normal structures like ribs and clavicles. Diffuse abnormalities can become more prominent if we are able to visualize these images without normal anatomy. Bone suppression images (BSI) can be generated either by dual-energy imaging or by applying post-processing techniques on CXR to suppress bony structures. Dual-energy uses images acquired at different energy levels to highlight either bone or soft tissue.[1] The images can be aquired by exposing the patient once (single-shot technique) or twice (dual-shot technique). BSI are also created using software algorithms that process image data and automatically remove bone structures. Various computer algorithms have been developed towards automatic segmentation and suppression of bony structures- ribs[2,3] and clavicles.[4,5] Clinical studies have shown improvement in reading performance of the radiologists for detection of lung nodules with bone suppressed images.[6,7] Also several studies have shown improved automatic detection of interstitial lung diseases[8] and tuberculosis (TB)[9] by using different bone suppression techniques.

Detection of tuberculosis (TB) in CXR is a difficult task due to its varied manifestations like opacification, pleural fluid, lymphadenopathy, blunt costophrenic angle, hilar elevation etc. The most common abnormalities are textural in the lung parenchyma like small and large diffused opacities, consolidation and nodular lesions.

Further author information: (Send correspondence to P.Maduskar@rad.umcn.nl)

CXR is being recommended by the World Health Organization (WHO) as one of the screening tools for prevalence surveys to exclude normal subjects from undergoing further expensive tests[10] . Hence, Computer aided detection (CAD) of tuberculosis on CXR is becoming an important research task due to its extensive use for screening and also lack of radiologists and skilled clinical officers in high TB incidence regions. A CAD prototype for detection of TB (CAD v. 1.08, Diagnostic Image Analysis Group, Nijmegen, The Netherlands)[11] was developed which computes a local textural abnormality score. In this work, region-wise analysis of abnormality scores is performed on normal and abnormal regions in original CXR and BSI to evaluate the benefit of BSI over original CXR. We use the bone suppression software package developed by Riverian (ClearRead Bone Suppression 2.4, formerly Softview 2.4, Riverain Medical, Miamisburg, Ohio), to generate BSI. Several studies have already used ClearRead software for nodule detection and showed improvement in radiologists performance.[6,12,13] These images are then used to train the CAD prototype for TB and region level abnormality scores are compared with corresponding abnormality scores of the original prototype.

2. METHODS

We train two CAD systems a. with original CXR, b. with BSI. A large database of digital CXR (Delft Imaging Systems, Veenendaal, The Netherlands) was acquired from two sites in Zambia and South Africa with high TB incidence rate. These images have been then manually annotated by a certified reader trained to read CXR according to the CRRS tuberculosis scoring system.[14] In case of doubt, the annotations were checked and validated by a chest radiologist. This database was then used to train and test the CAD systems which are briefly explained in the following sub-sections.

2.1 Original-CXR CAD

The research CAD prototype system was developed for the analysis of CXR from high burden countries in Sub-Saharan Africa. The prototype combines abnormality scores from various subsystems - textural abnormality detection system, clavicle detection system and shape abnormality detection system, at pixel and image level to come up with an abnormality score for the image.[11] Here we use only the textural abnormality detection subsystem, which is trained with manually annotated textural abnormalities. Features are based on moments of intensity distributions of Gaussian derivative filtered images at each pixel and its relative position inside the lung fields. These sampled pixels inside the segmented lung fields were then classified using a k-Nearest Neighbor classifier (k=15) to get a probabilistic abnormality score (Fig. 4, Column 2). These probabilistic labels are combined into one abnormality score for each image to label the image as normal/abnormal.

2.2 BSI CAD

BSI images were generated using ClearRead bone suppression package as mentioned in the above section. ClearRead is Food and Drug Administration (FDA) approved bone supression software for clinical use. ClearRead being a proprietary system, algorithmic details have not been disclosed. Using these BSI, another CAD system is trained in exactly the same way as the original CAD system. All the steps in the CAD system including automatic lung segmentation, feature extraction and classification are performed on BSI. Pixel level texture probability scores are generated inside the lung fields for each image for direct comparison with the pixel level probability scores of original CXR CAD system. (Fig. 4, Column 2 versus Column 4)

Flowchart of both the CAD systems is shown in Fig. 1. Original and its BSI image for a normal and abnormal image is shown in Fig. 2.

2.3 Region-wise Analysis

We perform region based analysis of normal and abnormal regions to evaluate the correctness and differences between the probabilistic output of original CXR and BSI CAD systems. Normal regions refer to automatically segmented unobscured lung fields in normal images with no present abnormalities. Abnormal regions refer to the manually delineated diffuse parenchymal abnormalities. These abnormal regions are further categorized into three subtlety categories - 1. subtle, 2. visible, 3. obvious (Fig. 4, Column 5). Probability scores are averaged over each region and individually analyzed for all the abnormality categories and normal regions.

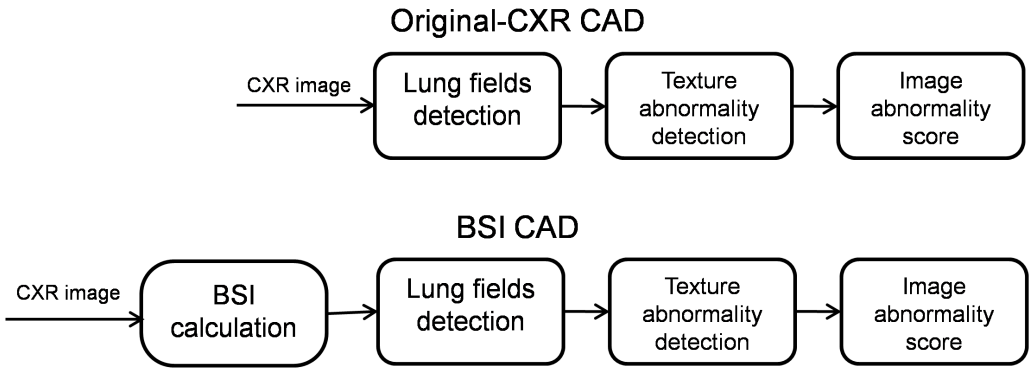

Figure 1. Flowchart of Original and BSI CAD system

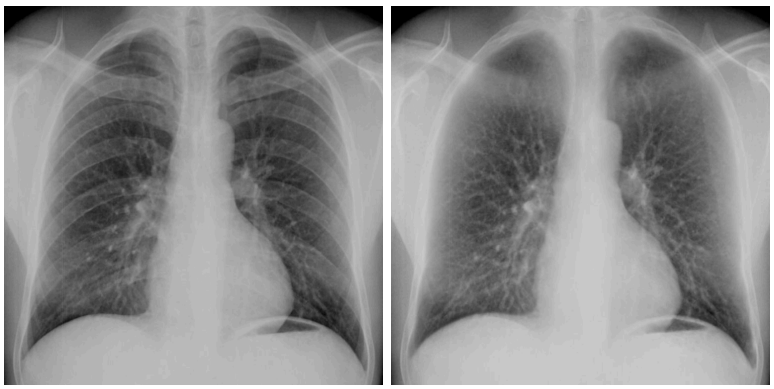

(a) Normal CXR image

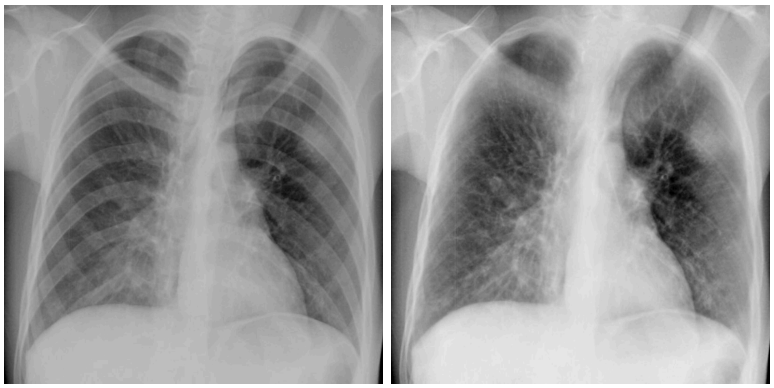

(b) Abnormal CXR image

Figure 2. Original CXR image and its corresponding BSI image

3. RESULTS

The CAD system is trained with randomly sampled normal pixels from 431 normal images and abnormal pixels from 434 abnormal images inside unobscured lung fields. The system is validated on an independent testset of 900 images containing 454 normal images. There are in total 454 normal regions and 1127 abnormal regions which consists of 280 (category 1), 527 (category 2) and 320 (category 3) abnormal regions, respectively. For

normal regions, BSI CAD produces slightly lower average abnormality scores than the original CAD, while for abnormal regions, the reverse is the case. The average abnormality scores and p-values are tabulated for normal and abnormal regions in Fig. 3 (b). p-values were computed using paired two-tailed t-tests.

From the box plots for abnormality scores of various regions (Fig. 3), it is apparent that BSI CAD system has lower scores for normal regions as compared to abnormal regions providing better discrimination than the original CXR CAD system. In Fig. 4, we observe improved probabilistic abnormality scores with less false responses for Category 1 and Category 3 abnormality image. For Category 2 abnormality image, we see some high response for abnormal regions in BSI output which is missing in the original CXR output. Normal image shows lower response for BSI than for the original CXR probabilistic abnormality score.

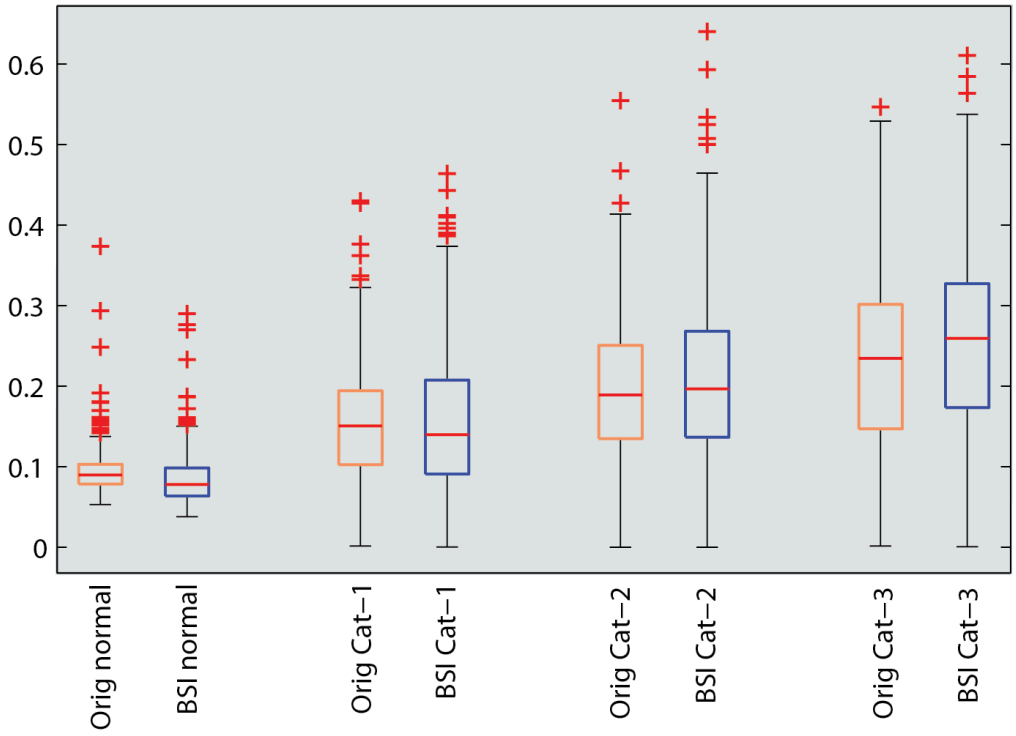

(a)

Categories	**Original CAD**	**BSI CAD**	**p-value**
Normal	0.094±0.027	0.085±0.032	5.6×10^{-19}
Category 1	0.155±0.073	0.156±0.089	0.73
Category 2	0.194±0.086	0.207±0.101	5.7×10^{-7}
Category 3	0.225±0.119	0.247±0.117	4.4×10^{-7}
All abnormals	0.193±0.097	0.206±0.108	2.2×10^{-11}

(b)

Figure 3. (a) Region-wise box plot of abnormality scores, Orig -Original CAD system, BSI- BSI CAD system, cat-1/2/3 - Abnormality categories (b) Average region abnormality scores and p-value(Original vs BSI) for normal and abnormal region categories

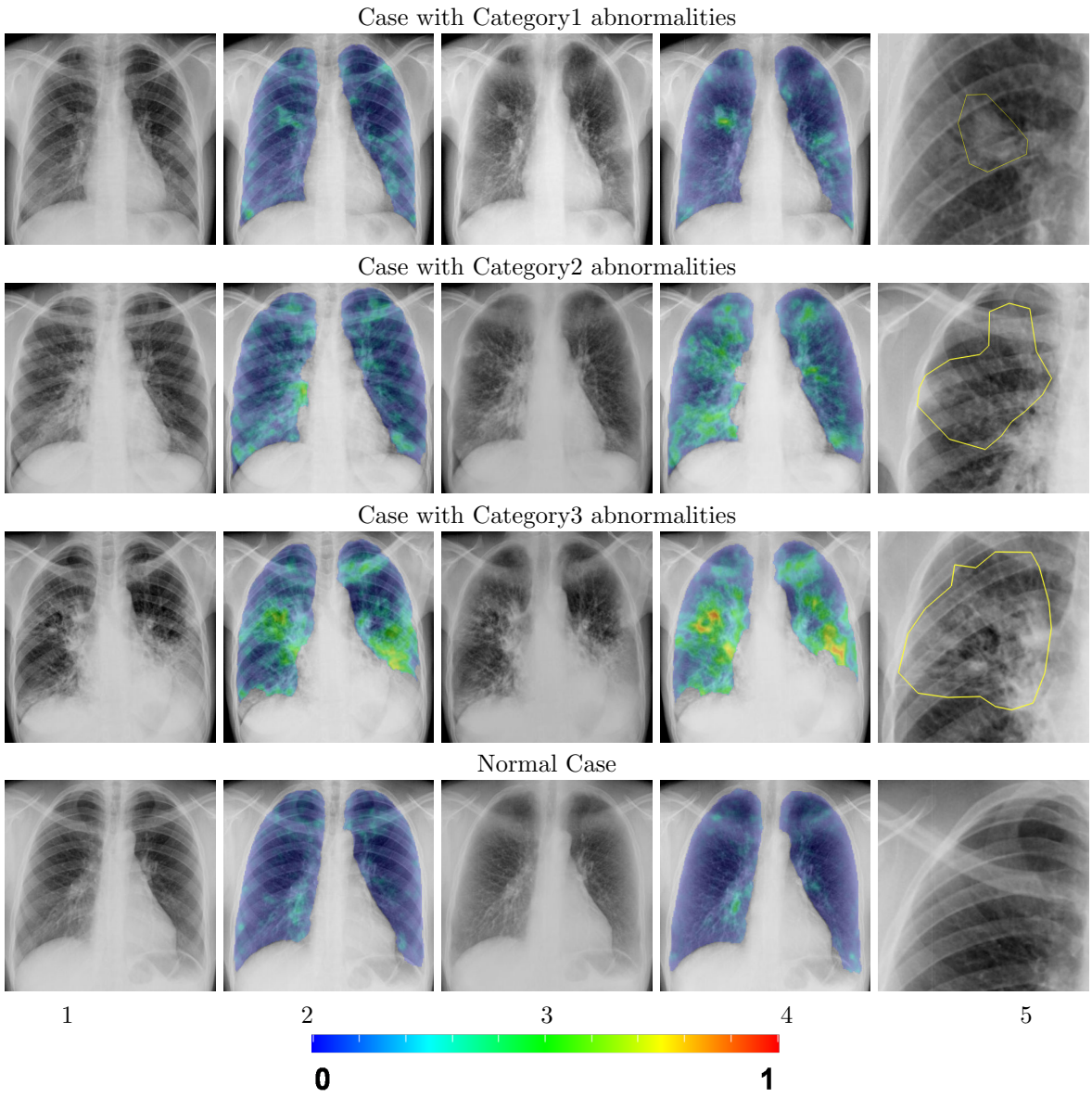

Figure 4. Column 1 and 2: Original CXR image and its abnormality score overlay, Column 3 and 4: Bone suppression image and its abnormality score overlay, Column 5: One of the annotated regions in the image for the corresponding abnormality category. Colorbar shows the color map used for overlay.

4. CONCLUSION AND FUTURE WORK

The use of bone suppression images leads to a small but significant improvement in training a CAD system for TB. We obtain improved detection of textural abnormalities and better discrimination between normal and abnormal regions. Improved abnormality scores at region level with BSI CAD system can assist in better visualization of automatically detected abnormal regions on a chest radiograph.

We have shown improvement with bone suppression images based on region based analysis. Category 1 abnormality images include very subtle abnormalities showing no significant difference with and without BSI. These subtle abnormalities need to be reconfirmed with an expert radiologist before investigating the cause of no improvement. This work needs to be extended to report the results at image level to see the impact of bone

suppression images on the performance of the CAD system for TB. Output of original and BSI CAD systems can be weighted and combined to further improve accuracy of the CAD system.

REFERENCES

[1] MacMahon, H., Li, F., Engelmann, R., Roberts, R., and Armato, S., "Dual energy subtraction and temporal subtraction chest radiography," *Journal of Thoracic Imaging* **23**, 77–85 (2008).

[2] Loog, M. and van Ginneken, B., "Bony Structure Suppression in Chest Radiographs," in [*Computer Vision Approaches to Medical Image Analysis*], *Lecture Notes in Computer Science* **4241**, 166–177 (2006).

[3] Suzuki, K., Abe, H., MacMahon, H., and Doi, K., "Image-processing technique for suppressing ribs in chest radiographs by means of massive training artificial neural network (MTANN)," *IEEE Transactions on Medical Imaging* **25**, 406–416 (2006).

[4] Yu, T., Luo, J., and Ahuja, N., "Shape regularized active contour using iterative global search and local optimization," in [*Computer Vision and Pattern Recognition, 2005. CVPR 2005. IEEE Computer Society Conference on*], **2**, 655–662 (2005).

[5] Hogeweg, L., Sánchez, C. I., de Jong, P. A., Maduskar, P., and van Ginneken, B., "Clavicle segmentation in chest radiographs," *Medical Image Analysis* **16**, 1490 – 1502 (2012).

[6] Freedman, M. T., Lo, S.-C. B., Seibel, J. C., and Bromley, C. M., "Lung nodules: improved detection with software that suppresses the rib and clavicle on chest radiographs," *Radiology* **260**, 265–273 (2011).

[7] Oda, S., Awai, K., Suzuki, K., Yanaga, Y., Funama, Y., MacMahon, H., and Yamashita, Y., "Performance of radiologists in detection of small pulmonary nodules on chest radiographs: effect of rib suppression with a massive-training artificial neural network," *American Journal of Roentgenology* **193**, W397–W402 (2009).

[8] Chen, X., Doi, K., Katsuragawa, S., and MacMahon, H., "Automated selection of regions of interest for quantitative analysis of lung textures in digital chest radiographs," *Medical Physics* **20**, 975–982 (1993).

[9] Hogeweg, L., Mol, C., de Jong, P. A., and van Ginneken, B., "Rib suppression in chest radiographs to improve classification of textural abnormalities," in [*Medical Imaging*], *Proceedings of the SPIE* **7624**, 76240Y1–76240Y6 (2010).

[10] WHO, "Tuberculosis prevalence surveys: a handbook." World Health Organization (2011).

[11] Hogeweg, L., Mol, C., de Jong, P. A., Dawson, R., Ayles, H., and van Ginneken, B., "Fusion of local and global detection systems to detect tuberculosis in chest radiographs," in [*Medical Image Computing and Computer-Assisted Intervention*], *Lecture Notes in Computer Science* **6363**, 650–657 (2010).

[12] Li, F., Hara, T., Shiraishi, J., Engelmann, R., MacMahon, H., and Doi, K., "Improved detection of subtle lung nodules by use of chest radiographs with bone suppression imaging: receiver operating characteristic analysis with and without localization," *American Journal of Roentgenology* **196**, W535–W541 (2011).

[13] Li, F., Engelmann, R., Pesce, L. L., Doi, K., Metz, C. E., and Macmahon, H., "Small lung cancers: improved detection by use of bone suppression imaging–comparison with dual-energy subtraction chest radiography," *Radiology* **261**, 937–949 (2011).

[14] Dawson, R., Masuka, P., Edwards, D. J., Bateman, E. D., Bekker, L.-G., Wood, R., and Lawn, S. D., "Chest radiograph reading and recording system: evaluation for tuberculosis screening in patients with advanced HIV," *International Journal of Tuberculosis and Lung Disease* **14**, 52–58 (2010).